npj | Clean Water

www.nature.com/npjcleanwater

ARTICLE OPEN

TiO_2 nanotube electrode for organic degradation coupled with flow-electrode capacitive deionization for brackish water desalination

Jihun Lim[1,3], Yong-Uk Shin[1,3], Aseom Son[1,2], Seok Won Hong[2] and Seungkwan Hong[1]✉

A photoelectrochemical (PEC) oxidation and flow-electrode capacitive deionization (FCDI) dual system was explored for the effective treatment of brackish water. Two anodic electrodes with electrochemically self-doped TiO_2 arrays (blue-mesh/ blue-plate TiO_2 nanotube arrays (BM-TNA & BP-TNA)) were fabricated by annealing at 600 °C, and applied for the treatment of a water system. Specifically, the BM-TNA confirmed lower electrical resistance and superior performance under multiple light source (UV-A, -B, and -C). Furthermore, the system generated powerful oxidizing reactive oxygen species (ROS), which were assessed via degradation of eight organic pollutants: bisphenol-A, 4-chlorophenol, cimetidine, sulfamethoxazole, benzoic acid, phenol, nitrobenzene, and acetaminophen. Decomposition efficiency was stable throughout a wide range of pH, and durability of the BM-TNA electrode was demonstrated through long-term operation. Concurrently, optimization of the FCDI process via key operational parameters (electrode mass loading, and applied voltage) achieved superior desalination performance, and specific energy consumption (SEC). In particular, increased mass loading enhanced charge transportation through the formation of stable charge-percolation pathways, leading to improved solution conductance. Finally, the feasibility of the dual system (PEC-FCDI) was verified through complete degradation of the organic substrates and successful desalination of the brackish water.

npj Clean Water (2022)5:7 ; https://doi.org/10.1038/s41545-022-00150-9

INTRODUCTION

The rising demand for freshwater due to the occurrence of water shortages worldwide has become an urgent challenge to be solved[1,2]. Only 5–6% of the multiple water bodies on the Earth contain directly usable freshwater, with the remainder consisting mostly of seawater[3,4]. Under these circumstances, increasing effort has been devoted to treating saline water in order to secure a safe supply of freshwater[5,6]. Saline water is typically classified based on its salinity concentration, which is commonly represented as total dissolved solids (TDS); seawater and brackish water have TDS values of >35,000 and 1000–10,000 mg L^{-1}, respectively[7]. Of these, brackish water has been observed to broadly contain organic pollutants, such as sulfamethoxazole (SMX), bisphenol-A (BPA), acetaminophen (AMP), 4-chlorophenol (4CP), nitrobenzene (NIB), benzoic acid (BA), phenol (PH), and cimetidine (CMT), which are mostly assumed to originate from various wastewater sources (such as industrial, medical, and aquaculture farms)[8]. These pollutants are transported throughout water bodies, causing severe disturbance to aquatic life (such as genetic variation and strong resistance)[9], and adversely affecting the human body upon consumption as they typically act as endocrine-disrupting substances[10,11]. Therefore, development and the successful application of technologies for the treatment of contaminated brackish water for drinking or domestic use is an essential matter[12].

Membrane desalination processes, such as reverse osmosis (RO) and nanofiltration (NF), have been highlighted as representative technologies for water treatment. Specifically, seawater reverse osmosis and brackish water reverse osmosis (BWRO) are widely used as typical seawater desalination processes, while BWRO and NF are applied for brackish water treatment. Accordingly, the NF process is expansively introduced in regions that rely heavily on brackish water to supplement its freshwater supply[13,14]. However, it is commonly reported that the NF membrane exhibits inadequate rejection of monovalent ions, and although performance for divalent ions and TOC may be competent, the removal of organics aggravates fouling of the membrane surface[15,16]. Furthermore, a recent study comprehensively reviewing the removal of organic compounds via the NF process presented that an extensive number of organic contaminants (i.e., PH, NIB) show extremely low rejection through the process[17]. Overall drawbacks of the technology include: (i) scaling by calcium and magnesium ions, (ii) fouling by suspended solids and organic matter, (iii) low removal efficiency of specific organic contaminants, and (iv) high maintenance cost with pressure being the driving force[18–21]. Hence, photoelectrochemical (PEC) oxidation coupled with flow-electrode capacitive deionization (FCDI) was introduced as an effective process for both the removal of organic pollutants and desalination to supersede the energy intensive yet deficient conventional membrane process.

Specifically, an electricity-driven PEC process using TiO_2-based nanotube arrays was investigated for organic contaminants removal. Photoelectrochemical (PEC) systems induce the activity of photoelectrocatalysts via external energy (such as UV light, visible light, and constant applied potential) to generate strong reactive oxygen species (ROS), such as hydroxyl radicals (•OH)[22–25]. The advantages of doping TiO_2 electrodes with nanotube arrays are due to the following: (i) increased specific surface area, (ii) open channel structure, and (iii) significant reduction in light loss[26,27]. In addition, TiO_2 catalyst materials are favorable owing to their non-toxicity, low cost, chemical stability, and durability[28].

[1]School of Civil, Environmental, and Architectural Engineering, Korea University, Seoul 136-701, Republic of Korea. [2]Water Cycle Research Center, Korea Institute of Science and Technology (KIST), Seoul 02792, Republic of Korea. [3]These authors contributed equally: Jihun Lim, Yong-Uk Shin. ✉email: skhong@korea.ac.kr

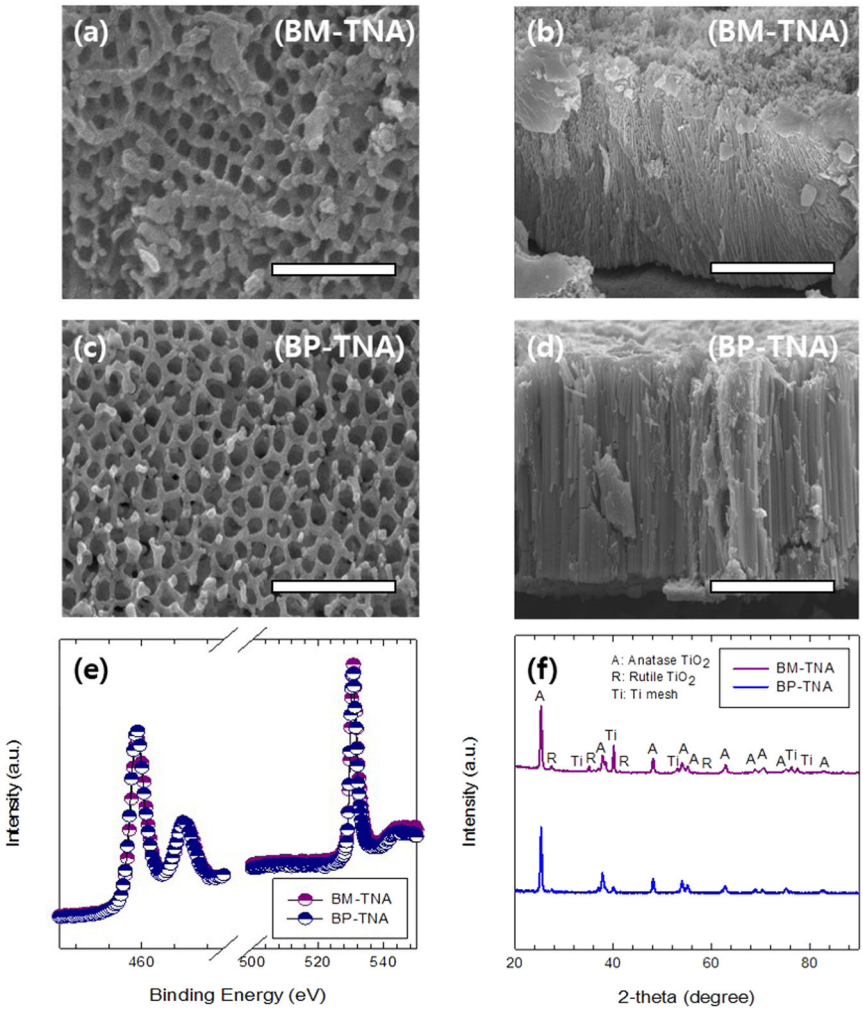

Fig. 1 Characterization of the BM- and BP-TNA electrodes via SEM, XPS, and XRD analyses. SEM images of **a**, **b** BM-TNA and **c**, **d** BP-TNA; **e** XPS signals and **f** XRD intensities. The length of the scale bars are as follows: **a**, **c** 500 μm; **b**, **d** 5 μm.

In conjunction with the PEC process for the degradation of organic pollutants, a subsequent deionization process is required for the desalination of brackish water. Among the various deionization systems, FCDI has attracted increasing interest as it is driven by electricity and can achieve desalination through continuous electro-adsorption of ions[29]. The FCDI technology has the following technical benefits over traditional capacitive deionization (CDI) and membrane capacitive deionization (MCDI) processes: (i) continuous and stable operation, (ii) significantly high adsorption capacity, and (iii) facile maintenance[30–32]. The technology uses flow electrodes (i.e., activated carbon particles) that pass through the flow channel of a current collector, and charged ions are transported through an ion exchange membrane upon the exertion of an applied voltage, which then adsorb to the electrode materials within the flow-electrode solution. To avoid water electrolysis, the applied voltage is typically limited to <1.23 V[32].

Further, the energetic efficacy of the FCDI system in comparison to the traditional membrane-based technologies in terms of brackish water treatment has been reviewed in previous literatures. One study reported the advantage of FCDI over RO within the boundary of producing permeate of freshwater concentration from initial feedwater salt concentrations of 2–3 g L^{-1} [33]. Another work evaluated the long-term operation of FCDI, and the system exhibited higher quality permeate than that typically produced from BWRO with an energy consumption of ≈0.3 kWh m^{-3}, which is economically feasible considering the typical 0.3–2.8 kWh m^{-3} energy consumption of the BWRO process[30,34,35]. A recent simulation also compared the energy consumptions of the capacitive process and BWRO, and reported an average volumetric energy consumption of 0.45 kWh m^{-3} for the capacitive system, which is highly comparable to the values reported by pilot and full-scale BWRO operation (0.5–7.7 kWh m^{-3})[32,36]. Moreover, the capacitive processes are low-pressure which decreases the demand for energy-intensive pumps, and since the systems perform as supercapacitors, they have the ability to store energy during the desalination phase which can be subsequently recovered[37].

In addition, FCDI operation is largely divided into two modes: short-circuited closed cycle (SCC) and isolated closed cycle (ICC). The SCC mode exhibits superior desalination performance and specific energy consumption (SEC) to the ICC mode[38], and is much more energy-efficient as automatic regeneration of the flow-electrodes via charge neutralization occurs within the external slurry reservoir even during the adsorption stage, which prolongs the requirement for the operation of a discharging phase[32]. In comparison, a previous study has reported that desorption under 0 V in the ICC mode does not guarantee the complete release of the adsorbed ions within the flow electrodes, and any additional discharging step under reverse voltage leads to further energy consumption[39]. Therefore, the SEC under the SCC mode has been

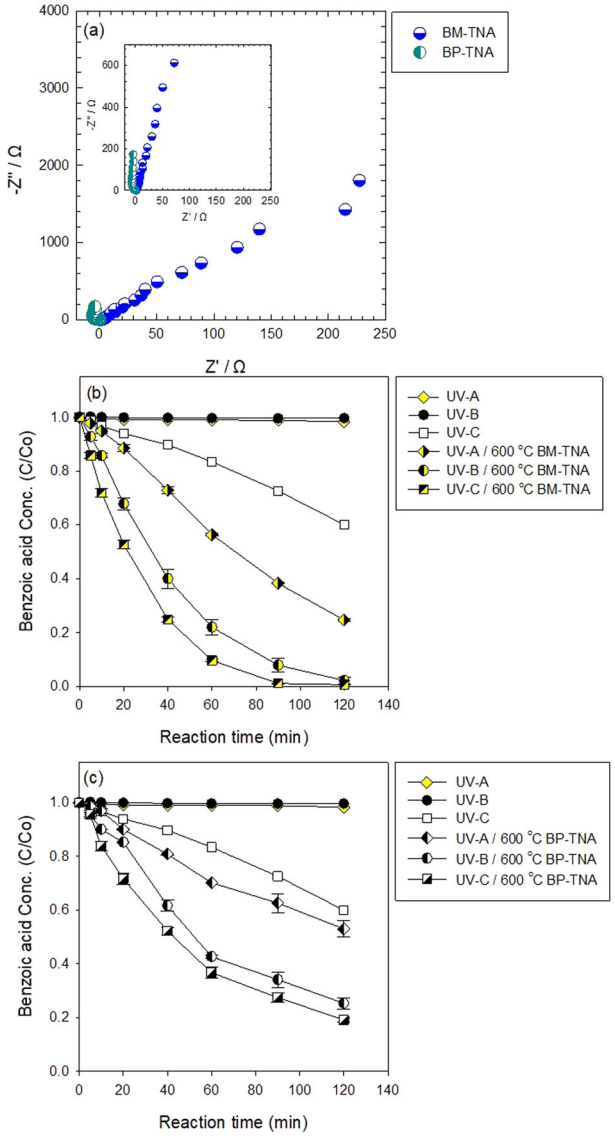

Fig. 2 Nyquist plot, and degradation of benzoic acid using BM- and BP-TNA electrodes under UV. a Nyquist plot (BM-TNA/BP-TNA) and **b**, **c** benzoic acid degradation by BM-TNA and BP-TNA photoelectrochemical processes under different forms of UV light ($[NaCl]_0 = 3000$ ppm; scan rate $= 50\ mV\ s^{-1}$ for LSV/CV; scan frequency = 100 kHz–10 mHz with 10 mV rms sinusoidal modulation versus open circuit potential for EIS; $[Benzoic\ acid]_0 = 0.1$ mM; constant voltage = 1 A; $pH_i = 7.0$).

evaluated to be only 20–50% of that under the ICC configuration[32].

Herein, we proposed a novel electrochemical dual process of PEC-FCDI for treating brackish water. Novel self-doped TiO_2 electrodes were fabricated under 600 °C, and applied to the treatment of brackish water for the first time in literature. Superiority of the catalysts was confirmed in comparison to our previous work[40], which investigated TiO_2 electrodes annealed at 450 °C, as higher annealing temperature led to higher catalyst activation[40]. Using the PEC system, eight pollutants present in brackish water were effectively mineralized using PEC electrodes (i.e., BM-TNA, BP-TNA) fabricated by the self-doping of Ti^{3+} (i.e., proton intercalation, $Ti^{4+} + e^- + H^+ \rightarrow Ti^{3+} + H^+$) via cathodic polarization. Also, BA was selected as a model substrate to confirm the formation of hydroxyl radicals by exploring the effect of radicals on the substrate to produce its oxidizing agent in the form of 4-hydroxylbenzoic acid (4-HBA) via hydroxylation. Concurrently, the presence or absence of radicals in the system was investigated by BPA degradation based on the scavenger effect with and without tert-butanol. In addition, the optimization of the FCDI operation was assessed under various flow-electrode mass loading and applied voltage conditions. The treatment performance indicated excellent salt adsorption capacity (SAC) and salt adsorption rate (SAR) in terms of energy efficiency. Finally, the feasibility of the dual system was confirmed through the complete decomposition of the target organic compounds from the feed solution by PEC pre-treatment, and exceptional deionization achieved by the post-FCDI system.

RESULTS AND DISCUSSION

Characterization of self-doped BM-TNA and BP-TNA electrodes

Figure 1(a) and (b) show the horizontal and cross-sectional FE-SEM images of the growth shape of the self-doped BM-TNA after annealing on a Ti mesh at 600 °C. The structure of the open TiO_2 nanotube array exhibited approximate outer and inner diameters of 138.0 and 75.3 nm, respectively, and a length of 9.7 µm. Similarly, Fig. 1(c) and (d) show the FE-SEM images of the self-doped BP-TNA annealed at 600 °C on a Ti plate. The results suggested that the anodization potential and annealing temperature were the key parameters in determining the crystallographic structure of the TiO_2 surface during the synthesis of BM-TNA and BP-TNA. In addition, the XPS results shown in Fig. 1(e) indicate Ti2p and O1s peaks with high binding energy. According to the visualization, the peaks for Ti2p and O1s were equally identified at 459.5 eV and 530.75 eV, respectively, for both the BP-TNA and BM-TNA electrodes. Figure 1(f) shows that the anatase and rutile peaks as the crystal structure were annealed in the order of XRD. This structural aspect was described in a previous study[40], and anatase peaks formed at 300 and 450 °C. In addition, mixed peaks (i.e., anatase and rutile) were observed at 600 °C. The behaviors of the self-doped BM-TNA, BP-TNA were confirmed through the applied cathodic reduction followed by the anatase peak at 450 °C, and the anatase and rutile peaks at 600 °C for the TiO_2 surface structure according to the change in annealing of the catalyst. These self-doped materials had excellent photochemical efficiency at peaks consisting of anatase and rutile peaks, which hindered reconversion.

Effect of the novel catalyst and photoelectrochemical activity via UV-lights source

To explore the potential of the catalyst, we evaluated the oxygen evolution reaction (OER) properties by comparing the activities of the BM-TNA and BP-TNA catalysts, as shown in the electrochemical impedance spectroscopy (EIS) results (Fig. 2(a)). EIS analysis confirmed the occurrence of charge transfer, which was evaluated under an open circuit potential with an amplitude of 10.0 mV over a scan frequency of 100.0–10.0 kHz in brackish water (i.e., 3000 mg L^{-1}). The BM-TNA exhibited a much higher transfer resistance than the BP-TNA catalysts, indicating the rapidly induced electron transfer efficiency of the BM-TNA.

To further evaluate the capacity of the two catalysts, degradation performance of BA as a model substrate within the PEC system under UV-A, B, and C lamps with and without the BM-TNA and BP-TNA catalysts was investigated as shown in Fig. 2(b) and (c). When the organic substance was irradiated with only the UV lamps, BA was hardly decomposed under UVA/B, while degradation slightly increased under the UVC light (Fig. 2(a)). However, in Fig. 2(b) and (c), it was confirmed that the morphology of the anodic catalyst (i.e., BM-TNA, BP-TNA) accelerated the decay of BA, and efficiency was much more significant for BM-TNA with its large specific surface area.

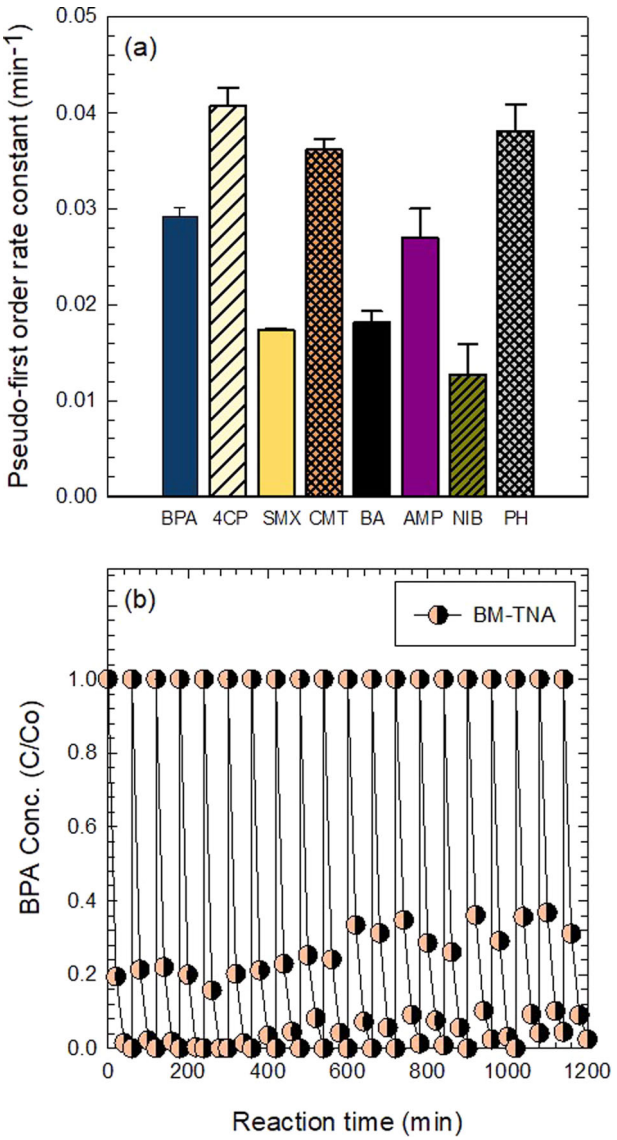

Fig. 3 Organic degradation via BM-TNA electrode, and evaluation of electrode stability. a Organic compound removal efficiency of BM-TNA under the photoelectrochemical system ($[\text{bisphenol-A}]_0$, $[\text{4-chlorophenol}]_0$, $[\text{sulfamethoxazole}]_0$, $[\text{cimetidine}]_0$, $[\text{benzoic acid}]_0$, $[\text{acetaminophen}]_0$, $[\text{nitrobenzene}]_0$, $[\text{phenol}]_0 = 0.1$ mM, $[\text{NaCl}]_0 = 3000$ ppm; $\text{pH}_i = 7.0$), and **b** repetition test of bisphenol-A decay ($[\text{bisphenol-A}]_0 = 10$ μM, $[\text{NaCl}]_0 = 3000$ ppm; $\text{pH}_i = 7.0$).

In the combined operation with the BM-TNA electrode annealed at 600 °C, degradation rate was significant with the reaction rate of the PEC system as follows: (k (UVC-PEC) $0.0444 \pm 0.0017\ \text{min}^{-1}$) > ($k$ (UVB-PEC) $0.0269 \pm 0.001\ \text{min}^{-1}$) > ($k$ (UVA-PEC) $0.0108 \pm 0.0004\ \text{min}^{-1}$). In contrast, degradation using the BP-TNA electrode equally annealed at 600 °C showed much lower results with the following reaction rates: (k (UVC-PEC) $0.0145 \pm 0.0004\ \text{min}^{-1}$) > ($k$ (UVB-PEC) $0.0119 \pm 0.0004\ \text{min}^{-1}$) > ($k$ (UVA-PEC) $0.0053 \pm 0.0001\ \text{min}^{-1}$). Significance of the novel BM-TNA catalyst was further confirmed through comparison with a similar BM-TNA electrode prepared at 450 °C (Supplementary Fig. 2). The novel electrode annealed at 600 °C exhibited greater mineralization efficiency, and the enhancement was distinguishable under all UV-A, B, and C lights. The measured energy consumption under UV-A, B, and C with a reaction time of 120 min was 0.035, 0.056, and 0.074 kWh, respectively.

The quenching effect of the BM-TNA catalyst in the presence of saltwater was also confirmed, as shown in Supplementary Fig. 3(a). When excess methanol and tert-butanol were applied, a dynamic delay in BPA degradation by the BM-TNA was observed. The main oxidant tended to degrade under the influence of hydroxyl radicals during electrolysis, and tert-butanol is effective for eliminating $^{\bullet}\text{OH}$ k ($^{\bullet}\text{OH} + \text{tert-BuoH} = 6.0 \times 10^8\ \text{M}^{-1}\text{S}^{-1}$). However, in the PEC system without a scavenger, the decomposition of BPA was monitored, indicating that reaction with UV-A light induced the formation of hydroxyl radicals as a powerful oxidizing agent due to the nature of the OER catalyst. Concurrently, the decomposition efficiency was monitored with BA as the target compound to identify the strong ROS generated in the PEC system (Supplementary Fig. 3(b)). When BA was decomposed, the formation of by-product as 4-HBA was confirmed, and an excellent reduction in TOC was observed.

Removal of organic compounds and catalytic stability of the PEC system

The removal efficiencies of various organic pollutants in the PEC system were represented by pseudo-first-order rate constants, as shown in Fig. 3(a). Representative organic contaminants in brackish water were selected for investigation (i.e., BPA, 4CP, CMT, BA, PH, NIB, AMP, and SMX). The reaction rates of the organic pollutants in the system were as follows: (k (4CP) $= 0.0447 \pm 0.0019\ \text{min}^{-1}$) > ($k$ (PH) $= 0.0381 \pm 0.0028\ \text{min}^{-1}$) > ($k$ (CMT) $= 0.0361 \pm 0.0012\ \text{min}^{-1}$) > ($k$ (BPA) $= 0.0291 \pm 0.001\ \text{min}^{-1}$) > ($k$ (AMP) $= 0.0270 \pm 0.003\ \text{min}^{-1}$) > ($k$ (BA) $= 0.0181 \pm 0.0012\ \text{min}^{-1}$) > ($k$ (SMX) $= 0.0173 \pm 0.0002\ \text{min}^{-1}$) > ($k$ (NIB) $= 0.0127 \pm 0.0032\ \text{min}^{-1}$). The PEC oxidation efficiencies, including aromatic compounds (such as electron-donating group (EDG) and electron-withdrawing group (EWG)) for BM-TNA catalysts exhibit different substrate specificities[41,42]. For instance, the phenolic compounds of EDG more easily released protons into the solution under $^{\bullet}\text{OH}$- induced oxidation, and were more susceptible to PEC anodization[43,44]. Specifically, the positive redox potential of 4CP exhibited faster degradation than PH (+0.86 V_{NHE} for PH versus +0.8 V_{NHE} for 4CP), which may contribute to the significant resistance against the oxidation[45,46]. In contrast, the EWG (i.e., BA and NIB) dynamically hindered the degradation of BA and NIB via benzene ring substitution[24].

The stability and durability of the BM-TNA catalyst system were evaluated via 20 repeated BPA degradation cycles in the PEC cell (Fig. 3(b)). The results indicate the long-term stability of the catalyst through the similar decomposition efficiency to the initial value of BPA when operating continuously at an initial pH of 7 for 20 h. In addition, the catalysts annealed at 600 °C maintained the initial color (i.e., blue) of the photocatalyst activity electrode. This result is linked to Supplementary Fig. 4, in which the BPA removal efficiency of the PEC system was evaluated as a function of pH (pH 3–9). The efficacy of BPA at pH 3, 5, 7, and 9 were 99.3%, 94.4%, 93.9%, and 87.3%, respectively. This result suggests that the kinetic retardation and inhibition of radical formation of the PEC cell under alkaline conditions (above pH 9) increased the OH^- content of the aquatic system.

Evaluation of the FCDI process operation via deionization and SEC

The performance of the FCDI operation was evaluated under three carbon mass loadings (5, 10, and 15 wt%) and three applied voltages (0.5, 0.8, and 1.1 V), and was optimized based on the SEC. In FCDI, activated carbon plays the role of ion adsorption owing to its exceptional surface area, electrical conductance, and ideal adsorption isotherm[47]. Accordingly, a higher carbon mass loading in the flow-electrode solution increases the surface area available for ion adsorption. In addition, activated carbon particles act as a bridge for charge transportation. In an ideal homogeneous solution, in which the distribution of the activated carbon particles

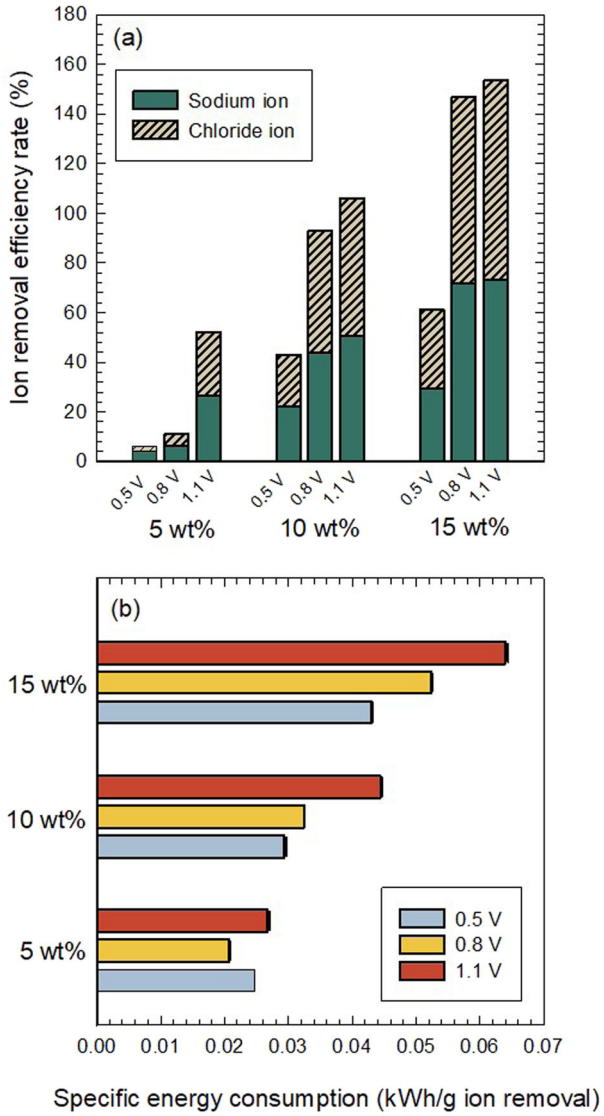

Fig. 4 Deionization performance and relative energy consumption of the FCDI system. a Ion removal efficiency, and **b** specific energy consumption of the flow-electrode capacitive deionization system (activated carbon mass loading = 5, 10, 15 wt%, applied voltage = 0.5, 0.8, 1.1 V, flow-electrode electrolyte = 1 M).

is even throughout the flow-electrode solution, charge transportation is also uniform with no fluctuation in the charge efficiency. However, flow-electrode solutions are heterogeneous and dynamic in nature, thus raising the issue of charge percolation. The deformation in the electrode material distribution during flow causes a decrease in the particle and charge connectivity[48]. Similarly, increasing the carbon mass loading allows the formation of strongly defined charge-percolation pathways, thereby improving the solution conductivity and accelerating charge transportation[49,50]. This relationship was confirmed to be consistent with previous studies that reported a positive correlation between the mass loading and conductivity of the flow-electrode solution[48].

Correspondingly, the ion removal efficiency of the system was enhanced as the mass loading and applied voltage increased, as shown in Fig. 4(a). Under an applied voltage of 0.5 V, the efficiency was, on average, seven-fold and eleven-fold higher when the carbon mass loading increased to 10 and 15 wt%, respectively. For 0.8 and 1.1 V, the efficiencies increased by approximately eightfold and thirteen-fold, and twofold and threefold, under 10 and 15 wt%, respectively. The obtained results were consistent with those of previous studies. One previous study reported a sharp increase in the desalting performance when the carbon mass loading was increased from 0 to 10 wt%[51], while another reported a similar trend in process performance as the mass loading increased from 20 to 25 wt%[52]. Ion removal was quantified in detail as shown in Supplementary Figs. 5–7, with (a) and (b) for the three figures representing the sodium and chloride ion concentrations in the permeate solution, respectively. A comparable reduction can be observed, with the slope of the concentration gradient becoming sharper as mass loading increased. (c) and (d) represent the ionic concentrations within the flow-electrode (slurry) solution, which were confirmed to increase as the ions within the feed stream adsorbed to the flow-electrode solution. The influences of the mass loading and applied voltage were further assessed via solution conductivity, SAC, and SAR, as shown in Supplementary Figs. 8–10. Regarding conductivity, a mass loading of 5 wt% resulted in nominal removal under all applied voltage conditions, with the maximum deionization reaching only ~20%. However, higher mass loadings of 10 and 15 wt% resulted in considerable enhancements. Quantitatively, the deionization performance under a mass loading of 10 wt% increased by 1.3-, 1.6-, and 1.8-fold under applied voltages of 0.5-, 0.8-, and 1.1 V, respectively, and by 1.4-, 1.8-, and 2.0-fold under a mass loading of 15 wt%. Similarly, increasing the two operational parameters enhanced the SAC, and the linear trend in SAR demonstrated the consistent performance of the FCDI system.

However, the parallel increase in viscosity and the decrease in solution fluidity are common major obstacles associated with increasing mass loading. Owing to the trade-off relationship, the loading in FCDI systems is commonly restricted to within 20 wt %[53–55] when no additional surface modification methods are followed for electrode material synthesis. Consistently, the mass loading condition in this study was limited to 15 wt%, and solution viscosity and clogging in the flow channel were not observed. As shown in Fig. 4(b), the validity of the mass loading and applied voltage was further assessed via SEC and quantified based on the total amount of ions removed during operation. The SEC followed a similar trend under all conditions, with the value increasing under higher loading rates. The change in the applied voltage followed comparable trends under mass loadings of 10 and 15 wt%. Despite the improvement in the deionization performance as the mass loading increased, as shown in Fig. 4(a), the reason for the higher SEC was the concurrent enhancement in the charge percolation of the system[52]. The strengthened electrical conductance and synchronous reduction in cell resistance led to the enhancement of current efficiency[56,57], resulting in a higher projected SEC. Specifically, the SEC values under a mass loading of 10 wt% were highly similar to those under 5 wt%. The changes in the values were below twofold for all applied voltage conditions, with the maximum being 1.6-fold. However, increasing the mass loading to 15 wt% increased the SEC values by 1.7, 2.4, and 2.5-fold under applied voltages of 0.5, 0.8, and 1.1 V, respectively. As the initial objective of the study was to obtain permeate within the suggested TDS range of potable water set by the World Health Organization or domestic water[58], the sequential two-adsorption operation was deemed sufficient to satisfy the standards based on the ion removal efficiency, as shown in Fig. 4(a). Therefore, a carbon mass loading and applied voltage of 10 wt% and 0.8 V were determined to be the optimal operational parameters, respectively. Comparably, a higher applied voltage (1.1 V) resulted in nominal changes in ion removal, with a much larger SEC. Similarly, a carbon mass loading of 15 wt% resulted in a higher deionization efficiency, which was also within a nominal range of ~1.2-fold with a much higher SEC.

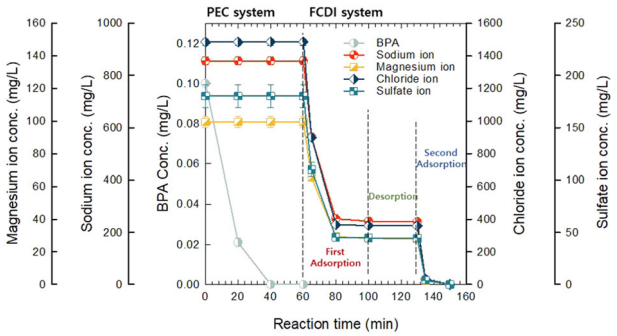

Fig. 5 Operation of the PEC-FCDI dual system. PEC-FCDI dual system (PEC: $[\text{bisphenol-A}]_0 = 0.1$ mM, $pH_i = 7.0$; operation time = 60 min) (FCDI: $[NaCl]_0 = 1947$ ppm, $[MgCl_2]_0 = 428$ ppm, $[Na_2SO_4]_0 = 278$ ppm, $pH_i = 7.0$; activated carbon mass loading = 10 wt%, applied voltage = 0.8/−0.8 V, flow-electrode electrolyte = 1 M; first-adsorption time = 40 min, desorption time = 30 min, second-adsorption time = 20 min).

Evaluation on the performance of PEC-FCDI dual process

The feasibility of the PEC-FCDI dual system was investigated by treating brackish water to produce organic contaminant-free permeate that meets the freshwater TDS standards. To investigate the efficacy of the system more accurately, the brackish water was prepared as a complex solution including multiple monovalent and divalent salts to reflect the composition of real brackish water as detailed in Supplementary Table 1. As shown in Fig. 5, the organic mineralization of BPA was evaluated at the PEC stage by measuring the TOC level. During the 60 min operation, an extremely sharp decrease in the TOC to 20% of the initial concentration was observed in the first 20 min. Subsequently, a three-log removal of BPA was monitored, with the final, complete degradation of the target pollutant occurring within 40 min of operation. No further formation of oxidation by-products was detected during the PEC process.

A subsequent FCDI stage was conducted for the purpose of deionization, and performance was evaluated based on the quantification of the removal of individual ions. During the first adsorption phase, a rapid decrease in the ion concentration generally occurred within 20 min. Specifically, the contents of sodium, magnesium, chloride and sulfate ions were reduced by 71, 72, 75.6 and 75.2%, respectively, indicating similar deionization efficiencies for both cations and anions. The adsorption rate eventually decelerated and reached a plateau as the pores of the activated carbon electrode became fully saturated with ions transported from the feed solution; thus, a desorption phase was required for the pores and charge balance of the system to recover to the initial state[38]. The desorption phase was conducted by reversing the applied voltage, and was operated for 30 min. The ions adsorbed in the micro-/ macropores of the electrode particles were discharged via electrostatic repulsion and transported across the ion exchange membranes to the feed stream. The ionic concentration of the flow-electrode slurry solution gradually decreased during the 30 min discharge operation, and all the ions adsorbed during the adsorption phase were discharged from the solution. After 30 min, the slurry solution was fully recovered for the operation of the second-adsorption phase. The final adsorption phase was conducted for 20 min with the permeate from the first adsorption phase as the feedwater solution. Under the low initial ion concentration, a similar rapid decline was observed, with almost two-log removal within minutes of operation, and complete deionization of the feedwater was ultimately achieved. Lastly, the energy consumption of the FCDI system was monitored, and the total combined SEC of the two-adsorption phases was 0.031 kWh g^{-1} ion removal, which was lower than that evaluated during the process optimization (Fig. 4), thereby further strengthening the feasibility of the technology for real water applications.

The treatment of brackish water for drinking or domestic use has mostly been conducted using brackish water RO or NF processes. However, critical drawbacks due to the low removal of trace organic pollutants, membrane surface fouling by the attachment of organics, and high energy consumption due to the pressure-driven nature of the technology indicate the limitations of the processes. In contrast, oxidation via the PEC system can achieve complete mineralization of trace organic compounds, while the subsequent deionization sequence of FCDI can attain ion desalination within the brackish water source under low energy consumption.

The novel self-doped BP-TNA and BM-TNA electrodes prepared by annealing at 600 °C revealed excellent charge transfer efficiencies, and effective degradation of eight model organic pollutants, with the BP-TNA showing superior performance. Organic mineralization was stably maintained at high levels throughout a wide pH range of 3–9, and a continuous experiment of seven repetitive cycles with uniform performance demonstrated the stability of the electrode. In addition, solution desalination was observed during the subsequent FCDI stage, and particularly, the increase in carbon mass loading improved charge-percolation pathways, which led to superior solution conductivity and charge transportation efficiency of the system.

The use of the hybrid PEC-FCDI system is expected to be a superior alternative to conventional processes. Owing to its exceptional performance and low energy consumption levels, the system is promising for practical application in the field of brackish water treatment for both potable or domestic use.

METHODS

Reagents

The following reagents were used without purification or treatment: BA (Sigma-Aldrich), 4CP (Aldrich), PH (Sigma-Aldrich), BPA (Aldrich), CMT (Sigma-Aldrich), AMP (Sigma-Aldrich), 4-hydroxybenzoic acid (Sigma-Aldrich). methanol (Sigma-Aldrich), *tert*-butanol (Sigma-Aldrich), sodium chloride (Sigma-Aldrich), sodium bicarbonate (Sigma-Aldrich), sodium carbonate (Sigma-Aldrich), perchloric acid (Sigma-Aldrich), phosphoric acid (Aldrich), and acetonitrile (J.T. Baker). All the chemicals used were of reagent grade, and ultrapure deionized (DI) water (>18 MΩ cm) produced from a Milli-Q water purification system was used to make the reagent solutions.

Feed solution

The organic compounds used for the PEC experiment included BA, SMX, BPA, AMP, 4CP, NIB, PH, and CMT in solutions prepared in ultrapure DI water (18.2 MΩ cm). To prepare synthetic brackish water (3 g L^{-1}) as a feed solution for the FCDI experiment, sodium chloride was added to DI water. Finally, the effluent from the PEC process was used as the feed solution for the FCDI experiment.

Flow electrode solution

The flow electrode slurry consisted of P-60 activated carbon powder with a Brunauer–Emmett–Teller (BET) surface area of 1311.7 $m^2 g^{-1}$ (Kuraray Co., Japan) in DI water, and three different activated carbon mass loading conditions were evaluated (5, 10, and 15 wt%). To ensure uniform suspension and maximization of the AC particle performance, the slurry solution was sonicated (model 350, Branson Sonic Power Co., USA) for 120 min, after which the BET surface area of the carbon particles increased to 2011.8 $m^2 g^{-1}$ (Supplementary Fig. 1). The electrolyte used for the slurry solution was 1 M sodium chloride.

Fabrication of self-doped BM-TNA and BP-TNA electrodes

Self-doped TiO_2 nanotube arrays (BM-TNA and BP-TNA) were prepared using a Ti mesh/plate and Pt foil (identical working area of 9.5 cm^2 and intergap distance of 1.0 cm) as the anode and cathode, respectively, via

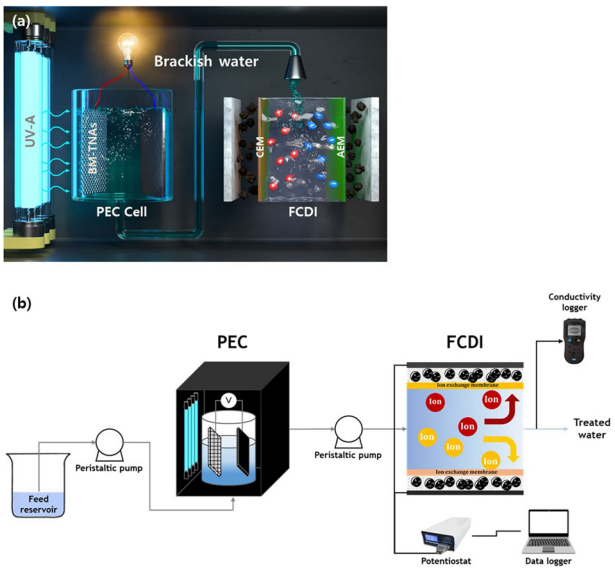

Fig. 6 Process schematic of the PEC-FCDI operation. a Graphic schematic of the dual PEC-FCDI system, and **b** detailed experimental process schematic of the overall system.

sequential anodization. In the first step, 45.0 V was applied using a DC power supply (TPM-1010, Toyotech Co., Republic of Korea) for 5 h in an ethylene glycol solution of 2.5 wt.% H_2O and 0.2 wt.% NH_4F. Additional anodization was then conducted at 10.0 V for 5 min to enhance the interfacial adhesion between the TNA layers and Ti mesh/plate. Following the successful fabrication of TNA layers on the Ti mesh/plate, anatase and rutile TNA were prepared by annealing at 600 °C (temperature elevation rate of 2.0 °C min^{-1}) for 1 h. BM-TNA and BP-TNA were finally produced through cathodic polarization by applying a constant current density of 16.7 mA cm^{-2} for 90 s using a potentiostat (WBCS3000M2, Wonatech, Republic of Korea) in a 0.1 M KH_2PO_4 solution (pH = 7.2). The electrode was then thoroughly rinsed with DI water to remove any residual chemicals. The term "BM (blue-mesh)-" and "BP (blue-plate)-" TNA was adopted because the surface color of the electrodes turned blue during the cathodic polarization step, and also a Ti mesh and Ti plate were used as the base anode material for the fabrication.

Experimental setup

The PEC organic pollutant degradation experiment was conducted using a three-electrode configuration, with the BM-TNA/BP-TNA, Ti mesh, and saturated Ag/AgCl as the working, counter, and reference electrodes, respectively. A rectangular cell (working volume of 90 mL) with a quartz window toward the light source was used as the reactor, which was placed inside a black box equipped with 4.0 W-UV-A (emission and peak emission wavelength of 350–400 and 352 nm, respectively; F4T5, Sankyo, Japan), UV-B (emission and peak emission wavelength of 280–260 and 310 nm, respectively; G4T5E, Sankyo, Japan), and UV-C (emission and peak emission wavelength of 100–280 and 254 nm, respectively; G4T5, Sankyo, Japan) lamps. All FCDI experiments were conducted using a custom-made cell, which was assembled in the order of PVC end plate, graphite current collector, cation exchange membrane, nylon spacer, anion exchange membrane, graphite current collector, and PVC end plate. The ion exchange membranes were commercially available products (Neosepta, ASTOM Co., Japan), and a potentiostat (WBCS3000M2, Wonatech, Republic of Korea) was used to apply a constant electrical potential to the FCDI unit. The feed and slurry solutions were consistently flown at flow rates of 5 and 35 mL/min, respectively, under the SCC mode. The conductivity of the permeate was recorded in real-time at the outlet of the FCDI cell using a conductivity meter (CDC401, Hach). A representative scheme of the overall operation is shown in Fig. 6.

Analytical methods

The physicochemical morphologies of the BM-TNA and BP-TNA were characterized by field emission scanning electron microscopy (FE-SEM; Quanta 250 FEG, FEI, USA), x-ray photoelectron spectroscopy (XPS; K-Alpha, Thermo Fisher Scientific, USA), and x-ray diffraction (XRD; New D8-Advance, Bruker-AXS, USA). The arrangement of the self-doped TNA layers was observed by FE-SEM at magnifications of ×10,000 and ×100,000, and XPS was used to examine the surface oxidation state of the BM-, anatase, and BP-TNA using Al Kα X-ray (hv = 1486.6 eV) as an excitation source. Adventitious carbon (248.8 eV) was used as a reference for binding energy calibration. XRD was used to identify the peaks of the surface crystalline structure with Cu Kα radiation (40.0 keV, λ = 0.154 nm). The concentrations of the organic pollutant compounds degraded during the PEC experiment were measured using a total organic carbon analyzer (TOC-V, Shimadzu, Japan) and high-performance liquid chromatograph (HPLC; Infinity 1260, Agilent, USA) equipped with a C-18 column (ZORBAX Eclipse XDB-C18, Agilent, USA) and UV/Vis detector (G1314F 1260VWD, Agilent, USA). The performance of FCDI (concentrations of ions such as Na^+, Cl^-) was evaluated by withdrawing samples from the unit at predetermined times using a 5 mL syringe, after which it was filtered through a 0.45 μm PTFE filter (Whatman) and analyzed using ion chromatography (IC, Dionex ICS-3000). The specific surface area of the P-60 activated carbon particles was analyzed following the BET method (BELSORP-MAX, Bel Japan Co., Japan).

FCDI performance and energy assessment

To evaluate the performance and energy consumption of FCDI, the following parameters were considered, along with their respective equations: (1) removal efficiency, (2) SEC, (3) SAC, and (4) SAR.

$$\text{Removal efficiency}\,(\%) = \frac{\Delta C}{C_i} \times 100 \tag{1}$$

$$\textit{Specific energy consumption}\,(kWh\ g^{-1}_{ion\ removal}) = \frac{V\int_0^t Idt}{\Delta CQt} \tag{2}$$

$$\text{Salt adsorption capacity}\,(\text{mg}\ g^{-1}) = \frac{Q\int \Delta Ct}{AC\ weight} \tag{3}$$

$$\text{Salt adsorption rate}\left(mg\ g^{-1}\ sec^{-1}\right) = \frac{SAC}{time} \tag{4}$$

where ΔC is the difference between the influent and effluent solution concentrations (mg/L), *V* is the applied potential, *I* is the current, *t* is the operating time, *Q* is the feed solution flowrate (mL/min), and 'AC weight' is the weight of the initial activated carbon powder used for the flow electrode.

DATA AVAILABILITY

Data generated and analyzed during this study are included in this published paper and its Supplementary Information files. Raw data used for this paper are available from the corresponding author within reasonable request.

Received: 30 August 2021; Accepted: 21 January 2022;
Published online: 04 March 2022

REFERENCES

1. Eliasson, J. The rising pressure of global water shortages. *Nat. N.* **517**, 6 (2015).
2. Tortajada, C. & van Rensburg. Drink more recycled wastewater. P. *Nat.* **577**, 26–28 (2020).
3. Alghoul, M., Poovanaesvaran, P., Sopian, K. & Sulaiman, M. Review of brackish water reverse osmosis (BWRO) system designs. *Renew. Sus. Energ. Rev.* **13**, 2661–2667 (2009).
4. Pan, S.-Y., Haddad, A. Z., Kumar, A. & Wang, S.-W. Brackish water desalination using reverse osmosis and capacitive deionization at the water-energy nexus. *Water Res.* **183**, 116064 (2020).
5. Schiermeier, Q. The parched planet: water on tap. *Nat. N.* **510**, 326 (2014).
6. Yang, Y., Pignatello, J. J., Ma, J. & Mitch, W. A. Comparison of halide impacts on the efficiency of contaminant degradation by sulfate and hydroxyl radical-based advanced oxidation processes (AOPs). *Environ. Sci. Technol.* **48**, 2344–2351 (2014).
7. Du, J. R. et al. Desalination of high salinity brackish water by an NF-RO hybrid system. *Desalination* **491**, 114445 (2020).

8. Du, X. et al. Boron-doped diamond (BDD) electro-oxidation coupled with nanofiltration for secondary wastewater treatment: Antibiotics degradation and biofouling. *Environ. Int.* **146**, 106291 (2021).
9. Hossain, A. et al. Occurrence, distribution, ecological and resistance risks of antibiotics in surface water of finfish and shellfish aquaculture in Bangladesh. *Chemosphere* **188**, 329–336 (2017).
10. Joseph, L., Heo, J., Park, Y.-G., Flora, J. R. & Yoon, Y. Adsorption of bisphenol A and 17α-ethinyl estradiol on single walled carbon nanotubes from seawater and brackish water. *Desalination* **281**, 68–74 (2011).
11. Westerhoff, P., Moon, H., Minakata, D. & Crittenden, J. Oxidation of organics in retentates from reverse osmosis wastewater reuse facilities. *Water Res.* **43**, 3992–3998 (2009).
12. Park, H., Park, Y., Kim, W. & Choi, W. Surface modification of TiO_2 photocatalyst for environmental applications. *J. Photoch. Photobio. C.* **15**, 1–20 (2013).
13. Ness, A. & MacNevin, D. Direct Potable Reuse as a Tool for Revitalizing Brackish Groundwater Desalination Facilities: Water Quality and Operations. *Fla. Water Resour. J.* **2**, 30 (2021).
14. Van der Bruggen, B. & Vandecasteele, C. Removal of pollutants from surface water and groundwater by nanofiltration: overview of possible applications in the drinking water industry. *Environ. Pollut.* **122**, 435–445 (2003).
15. Epsztein, R., Cheng, W., Shaulsky, E., Dizge, N. & Elimelech, M. Elucidating the mechanisms underlying the difference between chloride and nitrate rejection in nanofiltration. *J. Membr. Sci.* **548**, 694–701 (2018).
16. Epsztein, R., Nir, O., Lahav, O. & Green, M. Selective nitrate removal from groundwater using a hybrid nanofiltration–reverse osmosis filtration scheme. *Chem. Eng. J.* **279**, 372–378 (2015).
17. Shin, M. G. et al. Critical review and comprehensive analysis of trace organic compound (TOrC) removal with polyamide RO/NF membranes: mechanisms and materials. *Chem. Eng. J.* **427**, 130957 (2022).
18. AlTaee, A. & Sharif, A. O. Alternative design to dual stage NF seawater desalination using high rejection brackish water membranes. *Desalination* **273**, 391–397 (2011).
19. Lakretz, A., Mamane, H., Asa, E., Harif, T. & Herzberg, M. Biofouling control by UV/H_2O_2 pretreatment for brackish water reverse osmosis process. *Environ. Sci.-Wat. Res.* **4**, 1331–1344 (2018).
20. Nghiem, L. D., Coleman, P. J. & Espendiller, C. Mechanisms underlying the effects of membrane fouling on the nanofiltration of trace organic contaminants. *Desalination* **250**, 682–687 (2010).
21. Oatley-Radcliffe, D. L. et al. Nanofiltration membranes and processes: a review of research trends over the past decade. *J. Water Process. Eng.* **19**, 164–171 (2017).
22. Kim, J., Kim, C., Kim, S. & Yoon, J. RuO_2 coated blue TiO_2 nanotube array (blue TNA-RuO_2) as an effective anode material in electrochemical chlorine generation. *J. Ind. Eng. Chem.* **66**, 478–483 (2018).
23. Koo, M. S., Cho, K., Yoon, J. & Choi, W. Photoelectrochemical degradation of organic compounds coupled with molecular hydrogen generation using electrochromic TiO_2 nanotube arrays. *Environ. Sci. Technol.* **51**, 6590–6598 (2017).
24. Minakata, D., Li, K., Westerhoff, P. & Crittenden, J. Development of a group contribution method to predict aqueous phase hydroxyl radical (HO•) reaction rate constants. *Environ. Sci. Technol.* **43**, 6220–6227 (2009).
25. Wenk, J., Von Gunten, U. & Canonica, S. Effect of dissolved organic matter on the transformation of contaminants induced by excited triplet states and the hydroxyl radical. *Environ. Sci. Technol.* **45**, 1334–1340 (2011).
26. Cho, K. et al. Effects of reactive oxidants generation and capacitance on photoelectrochemical water disinfection with self-doped titanium dioxide nanotube arrays. *Appl. Catal. B-Environ.* **257**, 117910 (2019).
27. Ye, Y., Feng, Y., Bruning, H., Yntema, D. & Rijnaarts, H. Photocatalytic degradation of metoprolol by TiO_2 nanotube arrays and UV-LED: Effects of catalyst properties, operational parameters, commonly present water constituents, and photo-induced reactive species. *Appl. Catal. B-Environ.* **220**, 171–181 (2018).
28. Xu, X., Cai, J., Zhou, M., Du, X. & Zhang, Y. Photoelectrochemical degradation of 2, 4-dichlorophenoxyacetic acid using electrochemically self-doped Blue TiO_2 nanotube arrays with formic acid as electrolyte. *J. Hazard. Mater.* **382**, 121096 (2020).
29. Metzger, M. et al. Techno-economic analysis of capacitive and intercalative water deionization. *Energ. Environ. Sci.* **13**, 1544–1560 (2020).
30. Chung, H. J., Kim, J., Kim, D. I., Gwak, G. & Hong, S. Feasibility study of reverse osmosis–flow capacitive deionization (RO-FCDI) for energy-efficient desalination using seawater as the flow-electrode aqueous electrolyte. *Desalination* **479**, 114326 (2020).
31. Liu, E., Lee, L. Y., Ong, S. L. & Ng, H. Y. Treatment of industrial brine using Capacitive Deionization (CDI) towards zero liquid discharge–Challenges and optimization. *Water Res* **183**, 116059 (2020).
32. Shin, Y.-U., Lim, J., Boo, C. & Hong, S. Improving the feasibility and applicability of flow-electrode capacitive deionization (FCDI): Review of process optimization and energy efficiency. *Desalination* **502**, 114930 (2021).
33. Zhao, R., Porada, S., Biesheuvel, P. & Van der Wal, A. Energy consumption in membrane capacitive deionization for different water recoveries and flow rates, and comparison with reverse osmosis. *Desalination* **330**, 35–41 (2013).
34. Rosentreter, H., Walther, M. & Lerch, A. Partial Desalination of Saline Groundwater: Comparison of Nanofiltration, Reverse Osmosis and Membrane Capacitive Deionisation. *Membranes* **11**, 126 (2021).
35. Jeong, K. et al. Optimization of a nanofiltration and membrane capacitive deionization (NF-MCDI) hybrid system: Experimental and modeling studies. *Desalination* **493**, 114658 (2020).
36. Hand, S., Shang, X., Guest, J. S., Smith, K. C. & Cusick, R. D. Global Sensitivity Analysis To Characterize Operational Limits and Prioritize Performance Goals of Capacitive Deionization Technologies. *Environ. Sci. Technol.* **53**, 3748–3756 (2019).
37. Anderson, M. A., Cudero, A. L. & Palma, J. Capacitive deionization as an electrochemical means of saving energy and delivering clean water. Comparison to present desalination practices: Will it compete? *Electrochim. Acta* **55**, 3845–3856 (2010).
38. Luo, K. et al. Desalination behavior and performance of flow-electrode capacitive deionization under various operational modes. *Chem. Eng. J.* **389**, 124051 (2020).
39. He, C., Ma, J., Zhang, C., Song, J. & Waite, T. D. Short-circuited closed-cycle operation of flow-electrode CDI for brackish water softening. *Environ. Sci. Technol.* **52**, 9350–9360 (2018).
40. Son, A. et al. Persulfate enhanced photoelectrochemical oxidation of organic pollutants using self-doped TiO_2 nanotube arrays: Effect of operating parameters and water matrix. *Water Res.* **191**, 116803 (2021).
41. Lee, H. et al. Oxidizing capacity of periodate activated with iron-based bimetallic nanoparticles. *Environ. Sci. Technol.* **48**, 8086–8093 (2014).
42. Shin, Y.-U. et al. Electrochemical oxidation of organics in sulfate solutions on boron-doped diamond electrode: multiple pathways for sulfate radical generation. *Appl. Catal. B-Environ.* **254**, 156–165 (2019).
43. Anbar, M., Meyerstein, D. & Neta, P. The reactivity of aromatic compounds toward hydroxyl radicals. *J. Phys. Chem.-Us* **70**, 2660–2662 (1966).
44. Buxton, G. V., Greenstock, C. L., Helman, W. P. & Ross, A. B. Critical review of rate constants for reactions of hydrated electrons, hydrogen atoms and hydroxyl radicals (·OH/·O- in aqueous solution. *J. Phys. Chem. Ref. Data.* **17**, 513–886 (1988).
45. Jing, Y. & Chaplin, B. P. Mechanistic study of the validity of using hydroxyl radical probes to characterize electrochemical advanced oxidation processes. *Environ. Sci. Technol.* **51**, 2355–2365 (2017).
46. Reyter, D., Bélanger, D. & Roué, L. Nitrate removal by a paired electrolysis on copper and Ti/IrO_2 coupled electrodes–Influence of the anode/cathode surface area ratio. *Water Res.* **44**, 1918–1926 (2010).
47. Ntakirutimana, S., Tan, W., Anderson, M. A. & Wang, Y. Review-Activated Carbon Electrode Design: Engineering Tradeoff with Respect to Capacitive Deionization Performance. *J. Electrochem. Soc.* **167**, 143501 (2020).
48. Hatzell, K. B. et al. Direct observation of active material interactions in flowable electrodes using X-ray tomography. *Faraday Discuss* **199**, 511–524 (2017).
49. Nenashev, A. et al. Percolation description of charge transport in amorphous oxide semiconductors. *Phys. Rev. B.* **100**, 125202 (2019).
50. Park, H.-R. et al. Surface-modified spherical activated carbon for high carbon loading and its desalting performance in flow-electrode capacitive deionization. *RSC Adv.* **6**, 69720–69727 (2016).
51. Ma, J., He, C., He, D., Zhang, C. & Waite, T. D. Analysis of capacitive and electrodialytic contributions to water desalination by flow-electrode CDI. *Water Res.* **144**, 296–303 (2018).
52. Rommerskirchen, A., Linnartz, C. J., Müller, D., Willenberg, L. K. & Wessling, M. Energy recovery and process design in continuous flow–electrode capacitive deionization processes. *ACS Sustain. Chem. Eng.* **6**, 13007–13015 (2018).
53. Dahiya, S. & Mishra, B. K. Enhancing understandability and performance of flow electrode capacitive deionisation by optimizing configurational and operational parameters: a review on recent progress. *Sep. Purif. Technol.* **240**, 116660 (2020).
54. Porada, S. et al. Carbon flow electrodes for continuous operation of capacitive deionization and capacitive mixing energy generation. *J. Mater. Chem. A.* **2**, 9313–9321 (2014).
55. Zhang, C. et al. Flow Electrode Capacitive Deionization (FCDI): Recent Developments, Environmental Applications, and Future Perspectives. *Environ. Sci. Technol.* **55**, 4243–4267 (2021).
56. Liang, P. et al. Optimized desalination performance of high voltage flow-electrode capacitive deionization by adding carbon black in flow-electrode. *Desalination* **420**, 63–69 (2017).
57. Yang, S. et al. Flow-electrode capacitive deionization using an aqueous electrolyte with a high salt concentration. *Environ. Sci. Technol.* **50**, 5892–5899 (2016).
58. WHO. Guildelines for Drinking-water Quality. Report No. 9241548150 (2011).

ACKNOWLEDGEMENTS

This work was supported by the National Research Foundation of Korea (NRF) grant funded by the Korea government (MSIT) (No. NRF-2021R1A5A1032433).

AUTHOR CONTRIBUTIONS

J.L. and Y.U.S., the two main authors of the paper, contributed to the research design, PEC experiment and subsequent analyses, paper writing, and editing. A.S. and S.W.H. aided with the PEC research design. S.H. contributed to the guidance of the overall research as a corresponding author. Also, "J.L." and "Y.U.S." contributed equally to this work as both 'co-first authors'.

COMPETING INTERESTS

The authors declare no competing interests.

ADDITIONAL INFORMATION

Supplementary information The online version contains supplementary material available at https://doi.org/10.1038/s41545-022-00150-9.

Correspondence and requests for materials should be addressed to Seungkwan Hong .